Structural Insight into Enantioselective Inversion of an Alcohol Dehydrogenase Reveals a "Polar Gate" in Stereorecognition of Diaryl Ketones

Jieyu Zhou,[†] Yue Wang,[†] Guochao Xu,[†] Lian Wu,[‡] Ruizhi Han,[†] Ulrich Schwaneberg,[§] Yijian Rao,[†] Yi-Lei Zhao,[⊥] Jiahai Zhou,*[,‡] and Ye Ni*[,†]

[†]Key Laboratory of Industrial Biotechnology, Ministry of Education, School of Biotechnology, Jiangnan University, Wuxi, 214122 Jiangsu, China

[‡]State Key Laboratory of Bio-organic and Natural Products Chemistry, Center for Excellence in Molecular Synthesis, Shanghai Institute of Organic Chemistry, Chinese Academy of Sciences, Shanghai 200032, China

[§]Institute of Biotechnology, RWTH Aachen University, Worringerweg 3, 52074 Aachen, Germany

[⊥]State Key Laboratory of Microbial Metabolism, School of Life Sciences and Biotechnology, Shanghai Jiao Tong University, Shanghai 200240, China

S Supporting Information

ABSTRACT: Diaryl ketones are important building blocks for synthesizing pharmaceuticals and are generally regarded as "difficult-to-reduce" ketones due to the large steric hindrance of their two bulky aromatic side chains. Alcohol dehydrogenase from *Kluyveromyces polyspora* (*Kp*ADH) has been identified as a robust biocatalyst due to its high conversion of diaryl ketone substrate (4-chlorophenyl)(pyridine-2-yl)ketone (CPMK) with a moderate *R*-selectivity of 82% *ee*. To modulate the stereoselectivity of *Kp*ADH, a "polarity scanning" strategy was proposed, in which six key residues inside and at the entrance of the substrate binding pocket were identified. After iterative combinatorial mutagenesis, variants Mu-R2 and Mu-S5 with enhanced (99.2% *ee*, *R*) and inverted (97.8% *ee*, *S*) stereoselectivity were obtained. The crystal structures of *Kp*ADH and two mutants in complex with NADPH were resolved to elucidate the evolution of enantioselective

inversion. Based on MD simulation, Mu-R2−CPMK_{ProR} and Mu-S5−CPMK_{ProS} were more favorable in the formation of prereaction states. Interestingly, a quadrilateral plane formed by α-carbons of four residues (N136, V161, C237, and G214) was identified at the entrance of the substrate binding pocket of Mu-S5; this plane acts as a "polar gate" for substrates. Due to the discrepancy in charge characteristics between chlorophenyl and pyridine substituents, the pro-*S* orientation of CPMK is defined when it passes through the "polar gate" in Mu-S5, whereas the similar plane in wild-type is blocked by several aromatic residues. Our result paves the way for engineering stereocomplementary ADH toward bulky diaryl ketones and provides structural insight into the mechanism of stereoselective inversion.
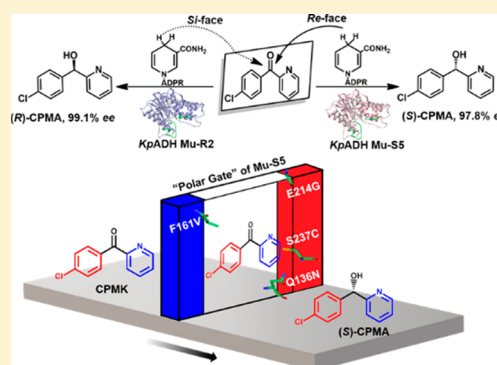
INTRODUCTION

Diaryl alcohols are important building blocks in the synthesis of pharmaceuticals.[1,2] Among them, (*S*)-(4-chlorophenyl)-(pyridin-2-yl) methanol [(*S*)-CPMA] is an important intermediate for synthesizing the antiallergy drug bepotastine (formerly designated as bepotastine besilate, (+)-(*S*)-4-{4-[(4-chlorophenyl)(2-pyridyl)methoxy]piperidino}butyric acid monobenzenesulfonate).[3,4] Bepotastine is a second-generation histamine H1 receptor antagonist possessing high binding selectivity and no side effects such as sedation and cardiotoxicity.[5] The synthetic method to produce bepotastine is patent-protected, and requires a resolving agent, (2*R*,3*R*)-2-hydroxy-3-(4-methoxyphenyl)-3-(2-nitro-5-chlorophenylthio)-propionic acid, which is expensive and not readily available. However, asymmetric reduction of (4-chlorophenyl)(pyridine-

2-yl)ketone (CPMK) is an alternative method for obtaining chiral intermediates of bepotastine. Due to the steric hindrance of two bulky aromatic substitutes, asymmetric reduction of diaryl ketones is often difficult for chemists and biologists.[6−8] Recently, a few studies on chemo- or bioreduction of diaryl ketones have been reported. Asymmetric transfer hydrogenation of CPMK in 40.8% *ee* (*R*)[9] and 60.6% *ee* (*S*)[10] has been achieved using ruthenium complex catalysts. *Sporobolomyces salmonicolor* carbonyl reductase (*Ss*CR) is the first heterologously expressed diaryl ketone dehydrogenase.[11] *Ss*CR and its mutant Q245P catalyzed the enantioselective reduction of (4-chlorophenyl)(phenyl)methanone at 78% *ee* (*R*) and
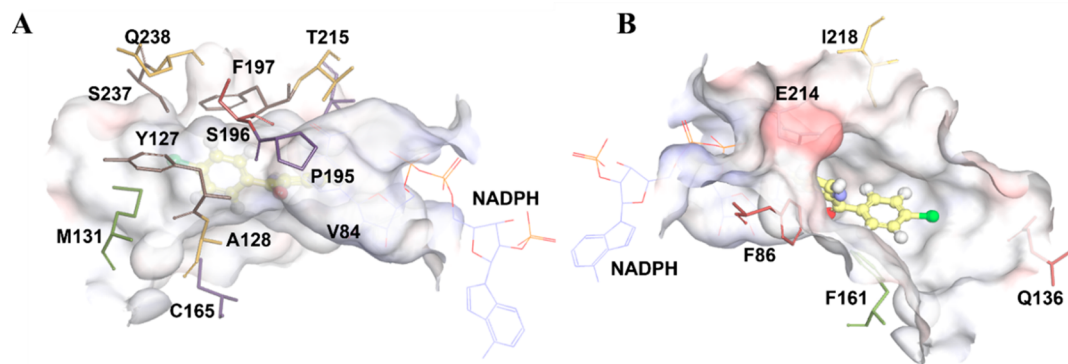
Figure 1. Residues chosen for polar scanning in the homology model of *Kp*ADH. (A) Residues within the substrate binding pocket. (B) Residues at the entrance of the substrate binding pocket. Residues are automatically assigned different colors.

76% *ee* (*S*), respectively.[12] *Cryptococcus sp.* whole-cell was employed as a catalyst for producing *S*-CPMA with excellent 99% *ee* in hydrophilic ionic liquid, whereas only 10 mM CPMK could be tolerated.[13] Apparently, the poor substrate tolerance and undesirable stereoselectivity of reported catalysts could not meet the requirements for pharmaceutical intermediates.

Alcohol dehydrogenases (ADHs, EC 1.1.1.X, X = 1 or 2) are nicotinamide adenine dinucleotide (phosphate) [NAD(P)$^+$]-dependent enzymes that catalyze the reduction of carbonyl compounds to their corresponding alcohols. The bioreduction of ketones is generally regarded as a green method that provides efficient access to optically active alcohols.[14] However, the application of ADHs is often hindered by their insufficient enantioselectivity and low activity.[15−17] According to Prelog's rule, hydrides are delivered from the *Re*- or *Si*-face in the asymmetric reduction of prochiral ketones to generate (*S*)- or (*R*)-configured alcohol products.[18] Engineering enzymatic enantioselectivity is often challenging due to the complicated stereorecognition mechanism.[19−22] Optimized codon usage in directed evolution experiments has emerged as a powerful means of engineering enantioselectivity.[23] For instance, using a triple code saturation mutagenesis, Sun and co-workers evolved highly *R*- and *S*-selective variants of TbSADH toward difficult-to-reduce ketones, such as tetrahydrofuran-3-one.[24] However, in most cases, semirational design based on crystal structure or a homology model is more suitable for enantioselectivity engineering due to the lack of high-throughput screening methods for chirality.[25] There have been several reports on engineering enantioselectivity of alcohol dehydrogenases, mainly focusing on aromatic ketones with only one aryl substitute. For instance, Patel and co-workers obtained five mutants with improved *ee* toward 4-phenyl-2-butanone from a comprehensive mutant library.[26] Li and co-workers found that aromatic and halogen substitutes played critical roles in stereoselectivity of SDRs (short-chain dehydrogenases/reductases), which was inverted from Prelog to anti-Prelog.[21]

Recently, an alcohol dehydrogenase from *Kluyveromyces polyspora* (*Kp*ADH) was discovered by genome mining. *Kp*ADH exhibited a moderate *ee* of 82.5% (*R*), with excellent substrate tolerance (>100 mM) toward diaryl ketones. A carbonyl group-dependent colorimetric high-throughput screening method was developed, and a beneficial variant S237A with improved *R*-selectivity of 96.1% was identified from a random mutagenesis library, indicating the evolvability of enantioselectivity.[27] Herein, we attempted to engineer

*Kp*ADH for inverted stereoselectivity from *R* to *S* toward diaryl ketone substrates. Key residues lining the substrate binding pocket were identified based on polarity scanning. Enantio-complementary variants were obtained after iterative combinatorial mutagenesis, which could be applied in the preparation of a variety of *S*- and *R*-diaryl alcohols. Crystal structures and computational data explained the stereoselective inversion of *Kp*ADH.

■ RESULTS AND DISCUSSION

Identification of Core Amino Acids. In our previous study, variant S237A was identified by random mutagenesis; this variant exhibited improved activity and enantioselectivity (96.1%, *R*) compared with WT (wild-type) *Kp*ADH.[27] This result suggests that protein engineering could be used to modulate its enantioselectivity. The homology model of *Kp*ADH was constructed based on the crystal structure of *Saccharomyces cerevisiae* NADPH-dependent methylglyoxal reductase GRE2 (PDB 4PVC) (EC 1.1.1.283).[28] *Kp*ADH possesses a superlarge substrate binding cavity with a calculated volume of 214.8 Å^3, while the solvent-excluded volume of CPMK is 159.8 Å^3 (computed by Accelrys Discovery Studio software)[29] based on its homology model. After eliminating the catalytic triad (S126−Y164−K168), 11 residues (V84, Y127, A128, M131, C165, P195, S196, F197, T215, S237, and Q238) within the binding site pocket (Figure 1A) and five residues (F161, F86, Q136, E214, and I218) at the entrance of the pocket (Figure 1B) were selected for further mutagenesis study.

Initially, we attempted to identify key residues responsible for enantioselective recognition. Screening semisaturation/saturation mutant libraries of 16 selected residues is, however, an enormous task even when a simplified NDT codon is used.[30] Based on the smallest alphabets proposed by Sun et al.,[31] saturation mutagenesis with single amino acid alphabets was attempted to reshape the binding pocket. All 16 residues were grouped based on their positions in the binding pocket, then each group of residues was simultaneously mutated to valine or alanine. However, most variants were inactivated after the mutation. This unsuccessful attempt indicates that the stereoselectivity of *Kp*ADH cannot be altered by simply reshaping the substrate binding pocket due to the large volume of its substrate pocket. A number of reports have demonstrated that "stereomatching" strategies such as alanine scanning are effective in identifying residues responsible for catalytic selectivity,[32,33] especially when the substrate contains sub-

stituents that differ substantially in steric hindrance.[34] In CPMK, chlorobenzene and pyridine groups are noncoplanar and could swing slightly around a pro-chiral carbon axis. As calculated by Discovery studio,[29] volumes of chlorobenzene and pyridine rings are estimated to be 111.2 Å^3 and 104.8 Å^3, respectively (Figure S1). The small difference in volume suggests that it is difficult to impact enantioselectivity by altering steric hindrance of residues alone.

Polarity Scanning of 16 Core Residues. In addition to steric effects, intermolecular forces (including ion-induced dipole force, ion−dipole force, hydrogen bonding, and van der Waals force) also play a key role in molecular recognition through ligand−protein binding.[35] Formation of intermolecular forces is closely related to the polarity of two molecules. The positive end of a polar molecule will attract the negative end of another molecule and thereby affect their position; thus the orientation of polar CPMK could be affected by its surrounding amino acids. Additionally, polarity at the entrance of the binding pocket could influence enzymatic selectivity or activity.[36] Therefore, a "polarity scanning" strategy was proposed to use typical polar/nonpolar amino acids as a sieve to eliminate residues with little effect on catalytic stereoselectivity by a single mutation. It is presumed that the polarity changes in the binding pocket could adjust the intermolecular force and thus affect the orientation of CPMK.

According to the hydropathy index of 20 amino acids,[37] arginine (−4.5) is a basic amino acid possessing the strongest polar side chain, followed by basic lysine (−3.9), and neutral asparagine (−3.5). Since the polarity of acidic and basic amino acids may be reduced or even eliminated by the formation of salt bonds, polar and neutral asparagine (−3.5) with a short side chain was selected as the "polar sieve". Simultaneously, valine (4.2) was considered an appropriate "nonpolar sieve" after comprehensive evaluation of its hydrophobicity, mobility, and steric hindrance.

Sixteen residues were subjected to "polarity scanning" by single mutation, and the effect of polarity change on stereoselectivity was determined using CPMK as a model substrate. The ee values of more than 90% or less than 75% were defined as the thresholds to select residues sensitive to polarity change. Six residues were obtained including Q136, F161, S196, E214, T215, and S237 (Figure S2). When these residues were mutated to polar Asn, decreased ee values were observed at Q136N (55.4%), E214N (33.4%), and S237N (73.4%); the same trend was evident when F161 and T215 were mutated into nonpolar Val. In addition, two markedly improved R-selective mutants S196V (98.2% ee) and E214V (92.8% ee) were identified. It is interesting that the stereoselectivity of E214V (92.8%, R) and T215V (43.8%, R) shows the opposite trend, even though the "inside site" 215 and the "entrance site" 214 are adjacent. These six residues exhibited a prominent influence on stereoselectivity and were thus subjected to further saturation and iteratively combinatorial mutagenesis.

Saturation Mutagenesis of Six Key Residues. To fully investigate the effect of Q136, F161, S196, E214, T215, and S237, saturation mutagenesis (SM) was performed using the NNK codon. Mutants that exhibited over 90% or less than 75% ee were selected for further iterative combinations (Table 1). For residue 136, over half of its SM library exhibited 75−80% ee. Among the others, Q136N (55.4%, R) and Q136S (68.6%, R) with decreased ee were selected. Despite the appreciable difference in the volume of Ser (99.1 Å^3) and Asn

Table 1. Saturation Mutagenesis of Six Key Residues for Evolving Enantioselectivity of *Kp*ADH

decreased/inverted variants	ee (%)	enhanced variants	ee (%)
Q136N	55.4	S196V	98.2
Q136S	68.6	S196W	96.1
S196G	47.5	S196P	93.5
F161V	72.6	E214V	92.8
E214G	−3.29	E214I	93.0
E214S	11.8	T215S	91.6
E214N	33.4	T215A	93.3
T215V	44.3	S237A	96.1
S237C	43.8	S237Y	93.9
S237N	73.4	S237W	94.3

(124.5 Å^3),[38] both variants showed a decrease in R-selectivity. A similar phenomenon was observed at sites 214 and 237. Variants E214G (3.3%, S), E214N (33.4%, R), and E214S (11.8%, R) exhibited a similar tendency in reversed stereoselectivity, whereas the stereoselectivity of S237A, S237T, and S237W was higher than 90%. T215S (91.6%, R), which was different from E214S (11.8%, R), was selected due to its enhanced R-selectivity; this was similar to the opposite trend observed with E214V and T215V. Residue S196 was picked for further saturation mutagenesis due to the excellent enantioselectivity of S196V (98.2% ee, R). Mutation of S196 to other nonpolar amino acids such as proline (93.5% ee, R) and tryptophan (96.1% ee, R) also resulted in improved ee, and reduced enantioselectivity was observed only for S196G (47.5% ee, R). For F161, all variants showed no significant improvement compared with WT, and F161V displayed the lowest R-selectivity of 72.6% (Figure S3).

Iterative Combinatorial Mutagenesis for Evolving Stereoselectivity. Iterative combinatorial mutagenesis (ICM) libraries were constructed using a data-based "Progressive Optimal Combination" (dPOC) approach. First, double-mutation libraries were constructed based on the 10 decreased/inverted single mutations listed in Table 1. For 95% coverage, theoretically only 111 transformants need to be screened for stereoselectivity inversion (Figure S4A). The best mutant, E214G/S237C (Mu-S2), led to pronounced inverted stereoselectivity in favor of the S-configuration of 51.8% ee. Other variants including S196G/E214S (32.3% ee, S), Q136N/E214G (34.2% ee, S), E214S/S237C (34.4% ee, S), and F161V/E214S (31.2% ee, S) were also identified, indicating positive synergistic effects among the selected residues (Table S1). Next, double mutants that exhibited S-preference were selected to construct triple mutagenesis libraries (Figure S4B). More than half of the mutants containing E214G or E214S reached over 80% ee (S), whereas mutants without these two mutations achieved merely 60% ee (S). Our results suggest that residue 214 plays an important role in the stereoinversion of *Kp*ADH, and synergistic effects of other residues are also indispensable. In progressive screening of quadruple mutagenesis libraries, Q136N/S196G/E214G/S237C (Mu-S4a) (92.2% ee, S) and F161V/S196G/E214G/S237C (Mu-S4b) (94.5% ee, S) were obtained (Figure S4C). After four rounds of ICM, Q136N/F161V/S196G/E214G/S237C (Mu-S5) with 97.8% ee (S) was attained. The optical purity of the S-CPMA product reached above 99% ee after recrystallization.[39]

Combinatorial libraries were also constructed based on the ten single mutants with enhanced stereoselectivity (Table 1). Fortunately, several excellent R-selective variants were
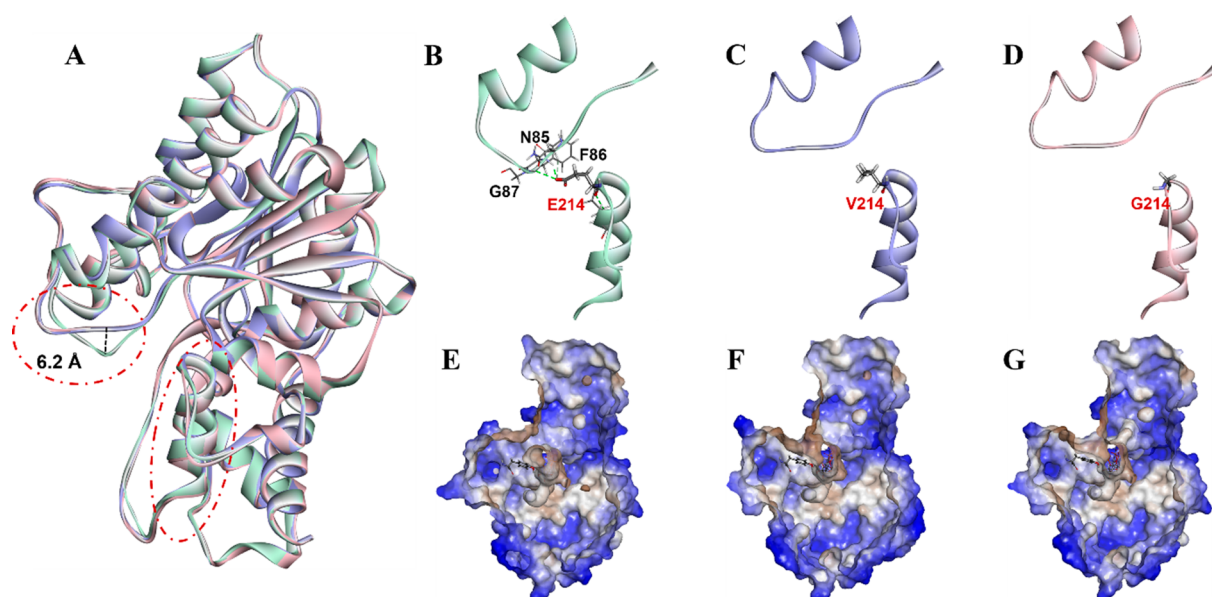
Figure 2. Overall crystal structures of WT (5Z2X), Mu-R2 (5ZED), and Mu-S5 (5ZEC). (A) 3D Structure alignment of WT (green), Mu-R2 (purple blue), and Mu-S5 (pink). Images B, C, and D represent detailed views of circled areas in image A: main interactions between loop 82−96 and site 214 in WT, Mu-R2, and Mu-S5, respectively. Images E, F, and G represent the solvent surface profiles of WT, Mu-R2, and Mu-S5, respectively.

identified in the first round of double mutagenesis (Figure S4D). Compared with moderate *R*-selectivity of WT (82.5%), the best variant, E214V/T215S (Mu-R2), exhibited over 99% *ee* (*R*) and was also selected for further investigation. It is noteworthy that E214V and T215S are not the best among single mutants with enhanced *R*-selectivity (Table 1). The excellent stereoselectivity of Mu-R2 could therefore be attributed to a synergistic effect.

**Crystal Structures of WT *Kp*ADH, Mu-R2, and Mu-S5.** To probe the molecular mechanism of stereoselective inversion, we crystallized WT, Mu-R2, and Mu-S5 of *Kp*ADH. After screening 1300 crystallization conditions, crystals were obtained only when NADPH was added. The structures of three protein−NADPH complexes were solved by molecular replacement using the protein structure of Gre2 (PDB 4PVC)[28] as a model and refined to resolutions of 1.98, 2.20, and 1.78 Å. The asymmetric unit of each variant consists of two monomers in the $P6_1$ space group (Table S2). The three-dimensional (3D) structure of *Kp*ADH displayed high similarity with *Ss*CR (PDB 1ZZE)[11] with an RMSD of 1.67 Å on main-chain atoms, despite their low sequence identity of 27%. The crystal structure of *Kp*ADH represents the first resolved structure of alcohol dehydrogenase with high catalytic efficiency and enantioselectivity toward diaryl ketones. The overall folding of *Kp*ADH is consistent with structures of other members of the SDR family.[11,25i,40] *Kp*ADH has two distinct domains. One is an NADPH binding domain consisting of a standard Rossmann motif of a large twisted *β*-sheet surrounded by seven *α*-helices, and the other is a variable C-terminal domain responsible for substrate binding. The NADPH molecule fits the electron density map perfectly in all protein−NADPH complexes.

Based on structure alignment, a significant difference in loop 82−96 of WT and its variants was noticed (Figure 2A). Compared with WT, a dislocation of the loop in Mu-R2 and Mu-S5 is represented by the position of an *α*-carbon at the F86 site, and the offset distance after the mutation was determined

to be 6.2 Å (Figure 2B−D). In WT, the carboxylic acid group of E214 could form hydrogen bonds with one of the loop residues among N85, F86, and G87, resulting in an attractive force on loop 82−96. This result suggests that the crystal of WT *Kp*ADH was obtained under closed-binding pocket status as the substrate could not enter the catalytic center when the loop was bound with E214. In Mu-R2 and Mu-S5, neither E214V nor E214G could serve as a hydrogen donor to bind the loop (Figure 2C,D). As shown in Figure 2E−G, the surface of the enzyme is hydrophilic, while the catalytic center is a strongly hydrophobic region. Variants Mu-S5 and Mu-R2 (Figures 2F,G) possess a semiopened substrate binding pocket, which renders them more easily able to accept bulky substrates with excellent affinity and catalytic efficiency.

Molecular Dynamic Simulations of Prereaction State. The prereaction states observed in computational simulations could reflect early stereoselective recognition of enzymes.[41] Based on the reaction mechanism of short chain dehydrogenase, Ser126 stabilizes the substrate, Tyr164 functions as the catalytic base, and the pK_a of the hydroxyl group of Tyr164 could be lowered by Lys168. The reaction is initiated by proton transfer from Tyr164−OH to the carbonyl oxygen atom of CPMK. Then, the hydrogen atom of NADPH is transferred to the carbonyl carbon, and the carbonyl group of CPMK is converted into a hydroxyl group.[42] Therefore, there were two distances that could be used to evaluate whether the enzyme−substrate complex could be developed into the prereaction state. One is defined by the distance between the carbonyl oxygen (O14) of CPMK and the H atom of Tyr164−OH, designated as $d(O14_{CPMK}-H9_{Y164})$, indicating the formation of the hydrogen bond and the protonation of CPMK. The other is defined by the distance between the carbonyl carbon (C7) of CPMK and the hydrogen atom (H4) at C4 of NADPH, designated as $d(C7_{CPMK}-H4_{NPH})$, indicating the process of nucleophilic attack (Figure S5). $d(O14_{CPMK}-H9_{Y164}) \leq 3.4$ Å and $d(C7_{CPMK}-H4_{NPH}) \leq 4.5$ Å could be used to represent formation of the hydrogen bond
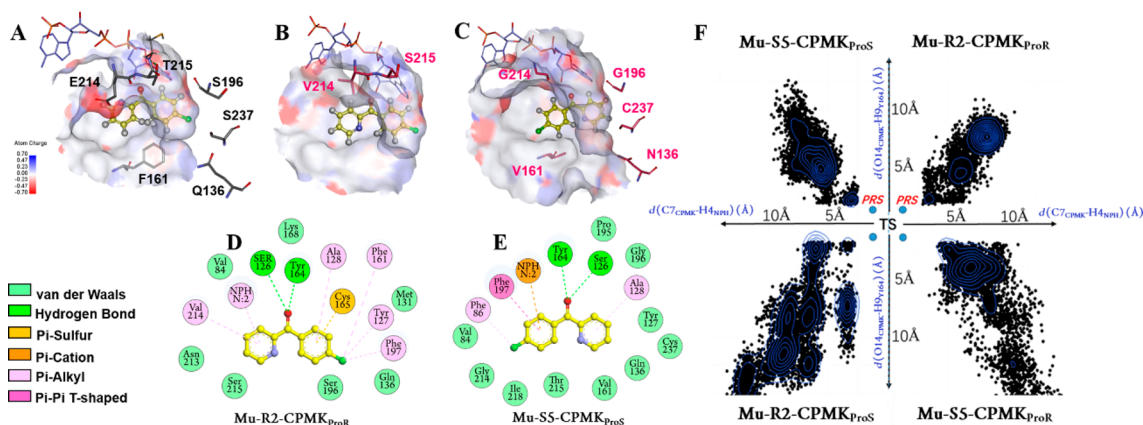
Figure 3. Docking poses of CPMK in WT (A), Mu-R2 (B), and Mu-S5(C). Interactions between CPMK$_{ProR}$ and Mu-R2 (D) and CPMK$_{ProS}$ and Mu-S5 (E) in prereaction states. Conformation maps of Mu-R2 and Mu-S5 in prereaction state simulations (F).
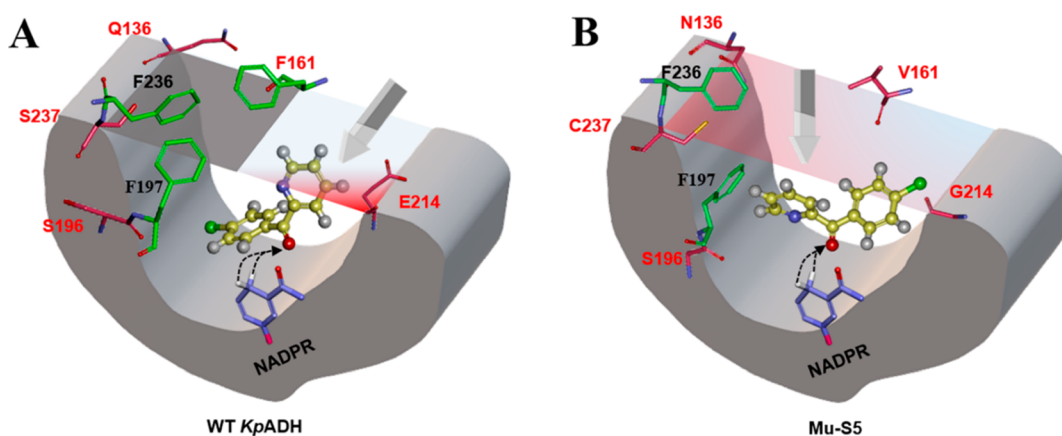
Figure 4. Typical catalytic conformations of (A) WT-CPMK$_{ProR}$ and (B) Mu-S5-CPMK$_{ProS}$ based on MD analysis; green sticks represent aromatic amino acids around CPMK; arrows indicate the entry direction of CPMK; the gray plane in part A represents the entrance blocked by aromatic amino acids of WT KpADH; the blue and red planes in (B) represent the polar entrance of Mu-S5; purple sticks represent NADPH, and black dashed lines indicate the direction of hydrogen attack; the mutation sites are marked in red.

and the process of hydride transfer, respectively.[43] Therefore, conformations meeting both constraints could be regarded as a sign of prereaction states. Additionally, the substrate in a prereaction state of the KpADH−CPMK complex could be defined as CPMK$_{ProS}$ and CPMK$_{ProR}$ according to the configuration of final alcohol products.

Docking studies using CDOCKER (Discovery Studio 4.0) were performed with WT, Mu-R2, and Mu-S5 with CPMK as a substrate. For WT, the energy of loop 82−96 needs to be lowered by loop refinement tools so that CPMK can be docked into the active site. Docking poses with the lowest CDOCKER energy (Table S3) were retained, and they were all in line with the experimentally observed stereoselectivity (Figure 3A−C). One interesting finding is that the substrate-binding pockets of Mu-R2 and Mu-S5 were more open than that of WT, whereas two variants showed higher stereoselectivity. A comparison of Figure 3, parts A and B, demonstrates that the polarity of WT and Mu-R2 varies greatly at the entrance. A less polar entrance of Mu-R2 is favorable for the preferential entry of chlorobenzene rings. Molecular dynamic simulations were then performed based on the docking studies. The orientation of CPMK$_{ProS}$ was observed in the stable prereaction states of Mu-S5, while CPMK$_{ProR}$ was observed in the stable prereaction states of Mu-R2 (Figure 3F). However, it is difficult to sustain a stable prereaction state of Mu-R2−CPMK$_{ProS}$ or Mu-S5−

CPMK$_{ProR}$. For Mu-S5, the distance between H4$_{NPH}$ and C7$_{CPMK}$ is too large for the nucleophilic reaction to proceed. For Mu-R2, it is difficult to form a stable hydrogen bond between Tyr164−OH and CPMK in the enzyme−substrate complex systems (Figure 3F). Remarkably, the proportions of "catalytic" conformations with both $d(O14_{CPMK}-H9_{Y164}) \leq$ 3.4 Å and $d(C7_{CPMK}-H4_{NPH}) \leq 4.5$ Å were 4.56% in Mu-R2−CPMK$_{ProR}$, more than eight times that observed in Mu-S5−CPMK$_{ProR}$ (0.52%). Similarly, the "catalytic" conformations in Mu-S5−CPMK$_{ProS}$ were 7.64%, approximately four times that observed in Mu-R2−CPMK$_{ProS}$ (1.84%). The above results demonstrate that Mu-R2−CPMK$_{ProR}$ and Mu-S5−CPMK$_{ProS}$ are more favorable in the formation of prereaction states to give corresponding (R)- and (S)-CPMA.

The structural characteristics of prereaction states of Mu-R2−CPMK$_{ProR}$ and Mu-S5−CPMK$_{ProS}$ were further studied. Major interactions of both systems were calculated as shown in Figure 3D,E, respectively. In Mu-R2−CPMK$_{ProR}$, the chlorobenzene ring of CPMK was mainly maintained through a π−alkyl hydrophobic interaction with A128, F161, Y127, and F197, while a similar π−alkyl hydrophobic interaction was formed between E214V and the pyridine group. In Mu-S5−CPMK$_{ProR}$, none of the five mutation sites had a direct interaction with the substrate (except van der Waals force), demonstrating that polarity change at these sites plays

Table 2. Kinetic Parameters of WT *Kp*ADH and Its Variants

	mutational sites	K_m (mM)	V_{max} (μmol·min^{-1}·mg^{-1})	K_{cat} (s^{-1})	K_{cat}/K_m (s^{-1}·mM^{-1})	ee (%)	config (R/S)
WT	none	0.410	17.9	11.8	28.9	82.5	R
Q136N	Q136N	0.160	17.2	11.4	71.5	55.4	R
E214G	E214G	0.520	11.1	7.32	14.1	3.29	S
S237C	S237C	0.204	41.3	27.3	134	42.9	R
S196G	S196G	0.922	8.78	5.81	6.30	47.5	R
F161V	F161V	1.08	30.9	22.6	20.9	72.6	R
Mu-S2	E214G/S237C	0.632	9.32	6.16	9.74	51.8	S
Mu-S3a	Q136N/E214G/S237C	0.861	10.2	6.76	7.85	88.0	S
Mu-S3b	Q136N/S196G/S237C	0.840	19.8	15.8	18.8	79.2	S
Mu-S4a	Q136N/S196G/E214G/S237C	1.82	27.0	21.6	11.8	92.2	S
Mu-S4b	F161V/S196G/E214G/S237C	0.720	21.3	17.0	23.6	94.5	S
Mu-S5	Q136N/F161V/S196G/E214G/S237C	1.12	25.2	20.1	17.9	97.8	S
E214V	E214V	0.574	17.5	11.7	14.2	92.8	R
T215S	T215S	0.973	24.8	16.5	16.9	91.6	R
Mu-R2	E214V/T215S	0.702	21.3	14.2	20.3	99.2	R
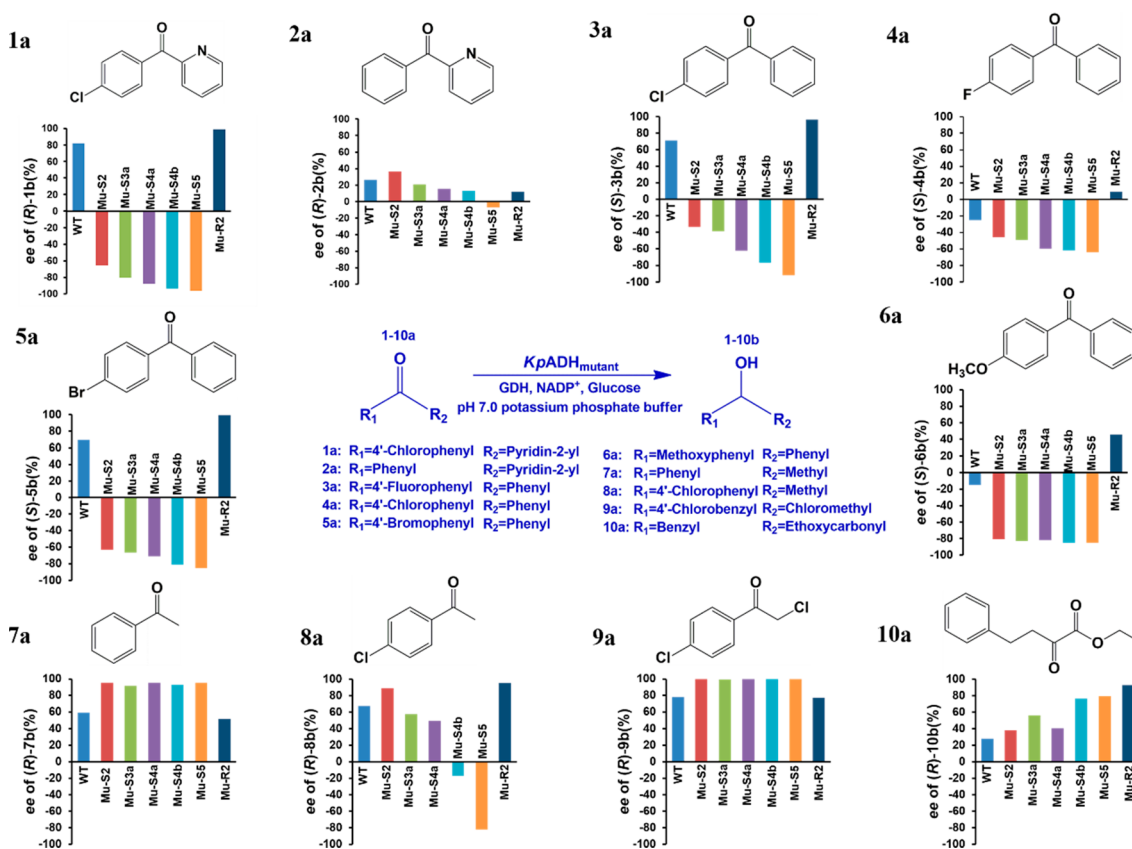
Figure 5. Enantioselectivity of WT *Kp*ADH and its variants in the asymmetric reduction of various aromatic ketones **1a−10a**.

significant roles in substrate recognition while a hydrophobic interaction is important for the formation of a stable prereaction.

Constrained MD Simulations Analysis Reveals Evolution of Stereoselective Inversion. To better understand the evolution of stereoselective inversion, constrained MD simulations with prereaction conformations of WT−CPMK$_{ProR}$, Mu-R2−CPMK$_{ProR}$, and Mu-S5−CPMK$_{ProS}$ as initial input were performed. Harmonic restraint was created on O14$_{CPMK}$, H9$_{Y164}$, and C4$_{NPH}$ to allow certain freedom in space, and thereby reduced computational time. After MD simulation, average conformations of three protein−ligand complexes were extracted and analyzed (Figure S6). The

polarity change at E214V made a major contribution to the stereoselective improvement as discussed above. The calculated total electrostatic interaction between site 214 and CPMK was −6.60 kcal/mol for WT−CPMK$_{ProR}$ (E214) and −2.59 kcal/mol in Mu-R2−CPMK$_{ProR}$ (V214).

The mechanism of stereoselective inversion was explored by comparing average conformation of WT−CPMK$_{ProR}$ and Mu-S5−CPMK$_{ProS}$. For Mu-S5, a quadrilateral plane with a dihedral angle of 0.31° could be formed when connecting α-carbons of four mutation sites, N136, V161, C237, and G214 (Figure S7B). This plane has a special charge distribution due to the different polarities of these amino acids (Figure S7D). CPMK needs to traverse this plane to access the catalytic

center, which resembles passing through a "polar gate" (Figure 4B and Figure S7B). For CPMK, the chlorine-substituent endows the chlorobenzene ring electronegativity, while the surface of the basic pyridine ring on the other side of the carbonyl group was positively charged. The catalytic orientation of CPMK is presumed to be defined when traversing the "polar gate", due to its electrostatic attraction and repulsion forces. In addition, an alkyl hydrophobic interaction between V161 and chlorine-substituent and a π−π interaction between Y164 and chlorobenzene rings could be formed (Figure S7B). The nonbinding interaction network formed by five mutation sites results in a prominent synergistic effect on the evolution of S-selectivity.

In WT, a similar quadrilateral plane consisting of Q136, F161, E214, and S237 is, however, blocked by several aromatic amino acids (F161, F197, and F236) (Figure 4A and Figure S7A). Therefore, only one side of the aromatic ring (mostly chlorobenzene) of CPMK could enter when approaching the catalytic center (Figure 4A and Figure S7C). Compared with Mu-S5, more nonbonded interactions could be formed in WT (Figure S8), which favors a stronger affinity and a lower K_m toward the substrate (Table 2). Based on calculation in Accelrys Discovery Studio (Figure S9), the biggest difference in nonbonded interaction energy between WT and Mu-S5 was observed at site 214, representing the importance of E214G in stereoselective inversion. In the average conformation extracted, nonbonded interactions could be formed between Y164, F161, F197, C165, and the chlorobenzene ring. In addition, π−alkyl hydrophobic interactions could form between chlorine and residue Y127 in the binding pocket. These results explain the R-selectivity observed for WT.

Enantioselectivity toward Various Aromatic Ketones. Enantioselectivity of WT KpADH and its variants (Table 2) toward 10 ketone substrates are illustrated in Figure 5 and Table S4. All combinatorial mutants, with either inverted or enhanced selectivity, showed a synergistic effect on all diaryl ketones except the halogen-free substrate 2a, for which poor stereoselectivity was observed. This result demonstrates that the para-substituents on the benzene ring are critical in the chiral recognition of enzymes. For 3a, the pyridine ring is replaced by a benzene ring. Although all combinatorial mutants showed similar selectivity as that of 1a, Mu-S5 and Mu-R2 exhibited slightly lower ee values of 91.7% (R-3b) and 96.4% (S-3b). Compared with 1a (CPMK), the reversed configuration of 3a is mainly due to the changes in group priority based on the Cahn−Ingold−Prelog rule.[18] The effect of various para-substituted benzene rings on enantioselectivity of KpADH was evaluated using 3a−6a. Although polarities and molecular volumes of these diaryl ketones are different, all substituents including halogens and methoxy are electron-withdrawing groups and show electronegativity. Variant Mu-S5 showed the same R-selectivity for all above diaryl ketones, demonstrating that polar interactions are the major factor in its stereorecognition. WT and variants with single mutations exhibited opposite selectivity in the reduction of 4a (F-) and 6a (CH₃O-) compared with that of 3a (Cl-) and 5a (Br-). To understand the effect of various substituents on stereoselectivity, physical properties of these diaryl ketones were measured using Gaussian software. Using 5a as a reference, there was a small difference in the dipole moments between 5a (2.95 D) and 4a (3.02 D); the difference in the volume of 5a (164.4 Å³) and 4a (147.5 Å³), however, was significant. In contrast, the volume of 6a (168.3 Å³) was close to that of 5a,

while its dipole moment (4.88 D) was clearly different from that of 5a. Inverted selectivity for these two ketones is most likely caused by the reduced space steric effect of 4a and enhanced polarity of 6a, which affect the intermolecular forces. In addition, docking results based on the crystal structure of WT show that sites F197 and Y127 can form π−alkyl hydrophobic interactions with the chlorine atom in 3a and the bromine atom in 5a. For 4a or 6a, however, no interaction between WT and the substituents (fluorine or methoxy) was observed (Figure S10), which may be responsible for the relatively lower enantioselectivity compared with 3a and 5a. Substrates 7a−9a are ketone substrates containing only one aryl group. For mutant Mu-S5, configurations of products 7b−9b were different. It was therefore presumed that para-chlorine substituents on benzene rings are critical for chiral recognition. Compared with 7a, the opposite orientation was observed for substrates 8a and 9a under a catalytic state. Molecular docking analysis showed that hydrophobic interactions could be formed between Y127 and chlorine as well as NADPH and the chlorobenzene ring for substrates 8a and 9a, which favors the formation of (S)-8b and (R)-9b (Figure S11). Mu-S3, Mu-S4a, Mu-S4b, and Mu-S5 exhibited excellent ee (>99%) toward 9a. As a β-aromatic ketone ester, 10a has been widely investigated as a substrate in biocatalysis.[44] All variants displayed the same R-selectivity as WT, and the highest ee value (92.5% ee) was attained by Mu-R2.

Synthesis of Optically Pure R- and S-CPMA. The gram-scale synthesis of R- and S-CPMA was carried out using lyophilized recombinant E. coli cells overexpressing KpADH variants (Mu-R2 or Mu-S5) and BmGDH for NADH recycling. In a preliminary study, substrate inhibition was observed at CPMK concentrations higher than 100 mM. Thus, substrate fed-batch culture was adopted for substrate loading of 500 mM. For Mu-R2, CPMK was added at 0, 0.5, 1, 1.5, 2.0, and 4.0 h. A complete conversion of CPMK was achieved in 6 h (Figure S12A), and 1.62 g R-CPMA was obtained at a high optical purity (99.1% ee, $[\alpha]_D^{25} = -118.4$).

For Mu-S5, extended substrate feeding intervals allowed a complete reaction due to the relatively lower catalytic efficiency of Mu-S5 compared with Mu-R2 (Figure S12B). After 24 h, 500 mM CPMK was fully converted, and 1.61 g of S-CPMA at excellent optical purity (97.6% ee, $[\alpha]_D^{25} = 117.1$) was obtained. NMR data and chiral HPLC chromatograms are shown in Figure S13.

Conclusions and Perspectives. Here, we attempted to engineer KpADH for inverted stereoselectivity toward diaryl ketone substrates. A "polarity scanning" strategy was proposed to identify key residues responsible for stereorecognition in the substrate binding pocket and entrance tunnel. Based on saturation mutagenesis of six key residues, iterative combinatorial mutagenesis was performed, and two excellent variants, Mu-R2 (99.1% ee, R) and Mu-S5 (97.4% ee, S), were obtained. Though KpADH variants with excellent R- and S-selectivity were obtained, the homology modeling is of limited use in revealing the mechanisms of stereoselective inversion.

The crystals of WT and two variants (Mu-S5 and Mu-R2) in complex with NADPH were resolved, and the structures were further analyzed by prereaction state analysis and constrained MD simulation. Based on computational data, polarity changes at the substrate entrance are the predominant factor for the increased enantioselectivity of Mu-R2. In MD simulation analysis, a "polar gate" with a special charge distribution was observed in Mu-S5, which is formed by N136, V161, C237,

and G214. Remarkably, a pro-S catalytic configuration of CPMK is defined when traversing the "polar gate". The energy calculation by MD simulation proved the importance of E214 in stereoselectivity alteration, which is consistent with the experiments. This study provides efficient approaches for engineering stereocomplementary alcohol dehydrogenases toward bulky diaryl ketones and elucidates its mechanism of stereoselective inversion.

■ MATERIALS AND METHODS

Microorganism and Chemicals. Recombinant *E. coli* BL21 (DE3) strains harboring pET28-*Kp*ADH and pET28-*Bm*GDH have been constructed in a previous study.[27] (4-Chlorophenyl)(pyridin-2-yl)methanone (CPMK), all other reagents and solvents of analytical grade, and biochemical reagents were obtained from Sinopharm Chemical Reagent Co. Ltd.

Mutagenesis. Cloning and recombinant expression of *Kp*ADH was performed as described in our previous study.[27] To engineer the enantioselectivity, polarity scanning using asparagine and valine as "polar sieve" residues were employed toward residues around substrate-binding pocket of *Kp*ADH. Variants were generated using whole-plasmid mutagenesis protocol. Saturation mutagenesis was then performed on beneficial sites using the NNK codon. Mutants exhibiting over 90% or less than 75% *ee* were subjected to further iterative combinatorial mutagenesis. Equal moles of mutant plasmids were mixed and amplified using whole-plasmid PCR with KOD high-fidelity polymerase. The PCR procedures were as follows: 95 °C for 2 min, followed by 15 cycles of 94 °C for 30 s, 55 °C for 30 s, and 68 °C for 2 min and 30 s. After *Dpn*I digestion at 37 °C for 30 min, the PCR products were transformed into competent *E. coli* BL21 (DE3) cells and plated onto LB agar plates supplemented with 50 μg/mL kanamycin.

Library Screening. Variant colonies were inoculated into 300 μL of LB medium containing 50 μg/mL kanamycin in 96-well plates and grown at 37 °C for 12 h. Then 50 μL of cell culture was transferred into 450 μL of fresh LB medium containing 50 μg/mL kanamycin and incubated for another 2 h. Enzyme expression was induced by addition of IPTG to a final concentration of 0.4 mM. After 5 h of incubation at 25 °C, cells were harvested by centrifugation, then lysed by addition of 1000 U of lysozyme and shaking at 37 °C for 1 h. The plates were centrifuged at $4000 \times g$ and 4 °C for 15 min, and 10 μL of supernatant was transferred to a 96-well plate. The activity was determined by adding 190 μL of enzymatic assay solution comprised of 1 mM CPMK, 100 mM potassium phosphate buffer (pH 7.0), and 1 mM NADPH. The decrease in absorbance of NADPH at 340 nm was monitored by a microplate reader (Biotek, USA).

Molecular Docking. The homology model of *Kp*ADH was built based on the crystal structure of *Saccharomyces cerevisiae* NADPH-dependent methylglyoxal reductase GRE2 (EC 1.1.1.283) (Protein Data Bank Code 4PVC),[28] which shares 53% amino acid sequence identity with *Kp*ADH. Molecular docking was performed using Discovery studio 4.0.[29] Receptor proteins were prepared by eliminating all bound water molecules. Hydrogen atoms were then added to the protein, which was optimized by applying a CHARMm force field.[45] The active pocket was defined as amino acid residues enclosed within a 5 Å radius sphere centered on a cavity. Amino acids in or near the active pocket were selected to create protein conformations and refine side chains. The obtained conformations with hydrogen bond interactions between carbonyl oxygen and Tyr164, as well as a less than 4.5 Å distance between carbonyl carbon and NADPH-C4 atoms were considered as reasonable.

Molecular Dynamic Simulations of Prereaction State. The initial coordinates used in the PRS (prereaction state) modeling were taken from the CDOCKER results. The parameters of NADPH were generated with the RESP[46] method and RHF/6-31*[47] calculation as in the literature,[48] and those of water molecules were assigned with the TIP3P model. The force field parameters of the CPMK substrate were prepared with the Antechamber package, and the general Amber force field (GAFF) and ff03.r1 force field were applied for the

proteins. The complexes were placed in a truncated octahedral box of water molecules, extending 8.0 Å along each dimension. The total of 11 counterions, Na^+, were added to neutralize the system. Then the systems were minimized by the steepest descent minimization of 1000 steps followed the conjugate gradient minimization of 9000 steps, heated from 0 to 300 K at constant volume in 50 ps, and equilibrated for another 50 ps without any restraints. After an additional 10 ns of NPT simulation, constraints of d(O14$_{CPMK}$−H9$_{Y164}$) and d(C7$_{CPMK}$−H4$_{NPH}$) were added by using a harmonic vibrational potential with a force constant of 500 kcal/(mol·Å^2) and the O···H and C···H balance distance at 1.7 Å. The distance-restricted systems were reminimized, heated, and equilibrated with the same procedure. Then the distance constraints were removed, and the PRS structures were re-equilibrated for the trajectory production. Finally, multiple 10 ns trajectories were collected for further PRS analysis. In the MD simulations, the Particle Mesh Ewald (PME) method was employed for long-range electrostatic interactions.

Constrained Molecular Dynamics Simulation. The simulations were executed in the simulation module of the Discovery Studio 4.0.[29] Conformations of WT−CPMK$_{ProR}$, Mu-R2−CPMK$_{ProR}$, and Mu-S5−CPMK$_{ProS}$ of the prereaction state were treated with CHARMm force field. Harmonic restraint was created at O14$_{CPMK}$, H9$_{Y164}$, and C4$_{NPH}$. Explicit solvent was applied to the system under periodic boundary conditions, and then two stages of steepest descent energy minimization were conducted. The system was heated from 0 to 300 K in 50 ps, and then a 1 ns equilibration process was performed to thermally equilibrate the molecules of the systems. The hydrogen bonds were fixed using the SHAKE algorithm during MD. Finally, a 20 ns MD simulation was performed on the whole system at 300 K.

Enantioselectivity of *Kp*ADH and Mutants toward Prochiral Ketones. Enantioselectivity of *Kp*ADH and mutants toward 10 prochiral ketones was determined by monitoring the reduction of these aromatic ketones in an NADPH regeneration system containing purified enzyme and glucose dehydrogenase (GDH) from *Bacillus subtilis*. The reaction mixture (500 μL) included 0.25 mM NADP+, 10 mM ketone/ketonic ester, 100 μg of purified mutant or WT *Kp*ADH enzyme, 15 mM glucose, and 2 U of GDH in 100 mM phosphate buffer (pH 7.0). After 6 h of reduction, the reaction medium was extracted with ethyl acetate. The *ee* value and concentration of produced alcohols were determined by HPLC or GC equipped with chiral columns as summarized in Table S5. The absolute configuration and identity of diaryl alcohol products were confirmed by comparing with refs 6 and 49.

Asymmetric Reduction of CPMK. Frozen cell pellets of *Kp*ADH variants and *Bm*GDH were mixed at ratio of 1:2 (25 U of *Kp*ADH variants and 50 U of *Bm*GDH) and suspended in sodium phosphate buffer (100 mM, pH 7.0). The reactions consisting of 10 mL of cell suspension mentioned above, 500 mM CPMK, and 1.5-fold glucose were performed in a 20 mL bioreactor at 30 °C and 200 rpm. The pH was automatically adjusted to 7.0 by titration with 1.0 M NaOH solution. The progress of the asymmetric reduction was monitored using Agilent 1100 HPLC equipped with a Chiralcel OB-H column (0.46 mm × 250 mm, 5 μm, Diacel, Japan). HPLC was performed at 254 nm using hexane/ethanol (95:5, v/v) as eluent at a flow rate of 1.0 mL/min and 30 °C.

Protein Crystallization. Crystals of WT and variants Mu-S5 and Mu-R2 in complex with NADPH were obtained at 18 °C using the sitting drop vapor diffusion technique, with the initial condition of mixing 1 μL of the 10 mg/mL protein sample and 1 mM NADPH with an equal volume of mother liquor (0.2 M ammonium acetate, 0.1 M HEPES, pH 7.0, 31% PEG 3350 for WT−NADPH complex; 0.2 M ammonium acetate, 0.1 M BIS-TRIS, pH 6.5, 27% PEG 3350 for Mu-S5−NADPH complex; 0.1 M BIS-TRIS, pH 6.5, 27% PEG3350 for Mu-R2−NADPH complex). Crystals grew up in about 3 days. Then, they were transferred into a cryoprotectant (reservoir solution supplemented with 10% (v/v) glycerol) and flash cooled in liquid nitrogen. All data were collected at the Shanghai Synchrotron Radiation Facility, Shanghai Institute of Applied Physics, Chinese Academy of Sciences, using beamline BL17B, BL18U. Data

processing and scaling were performed using the HKL3000 package.[50] All crystal structures were determined by molecular replacement method with PHENIX[51] using coordinates of *Saccharomyces cerevisiae* NADPH-dependent methylglyoxal reductase (PDB ID 4PVC, sequence identity is 53%) as the search model. PHENIX Phaser-MR (simple one-component interface) was used for building the initial model. Then initial model and phase information were transferred to native data set. Other parts of the structure were manually built in COOT[52] and iteratively refined in PHENIX Refine. In the final model, more than 99.8% of residues fell in the favored region in the Ramachandran plot, and the final Rwork/Rfree are 0.1589/0.1904, 0.1697/0.2150, and 0.1473/0.1780 for WT *Kp*ADH−NADPH, Mu-R2−NADPH, and Mu-S5−NADPH, respectively. Data collection and refinement statistics are listed in Table S2. The atomic coordinates of WT and variants Mu-R2 and Mu-S5 in complex with NADPH have been deposited in the Protein Data Bank (PDB) under accession numbers 5Z2X, 5ZED, and 5ZEC.

ASSOCIATED CONTENT

ⓢ Supporting Information

The Supporting Information is available free of charge on the ACS Publications website at DOI: 10.1021/jacs.8b08640.

> Selectivity data for additional mutants and data collection and refinement statistics for X-ray diffraction experiments (PDF)

> Crystallographic structures of WT, Mu-R2, and Mu-S5 *Kp*ADH in complex with NADPH (CIF)

AUTHOR INFORMATION

Corresponding Authors
*yni@jiangnan.edu.cn
*jiahai@mail.sioc.ac.cn

ORCID ⓞ
Ulrich Schwaneberg: 0000-0003-4026-701X
Yi-Lei Zhao: 0000-0003-4687-7847
Ye Ni: 0000-0003-4887-7517

Author Contributions
All authors have given approval to the final version of the manuscript.

Notes
The authors declare no competing financial interest.

ACKNOWLEDGMENTS

ABBREVIATIONS

MD, molecular dynamics; ICM, iterative combinatorial mutagenesis; dPOC, data based Progressive Optimal Combination; PRS, prereaction state

REFERENCES

(1) Devalia, J. L.; De Vos, C.; Hanotte, F.; Baltes, E. *Allergy* **2001**, *56*, 50−7.

(2) Schmidt, F.; Stemmler, R. T.; Rudolph, J.; Bolm, C. *Chem. Soc. Rev.* **2006**, *35*, 454−470.

(3) Roszkowski, A. P.; Govier, W. M. *Pharmacologist* **1959**, *1*, 60−78.

(4) Jen, W. S.; Truppo, M. D.; Amos, D.; Devine, P.; McNevin, M.; Biba, M.; Campos, K. *Org. Lett.* **2008**, *10*, 741−744.

(5) (a) Yato, N.; Murata, T.; Saito, N.; Sakai, A.; Kikuchi, M.; Tsuzurahara, K.; Marita, H. *Nippon Yakurigaku Zasshi* **1997**, *110*, 19−29. (b) Kida, T.; Fujii, A.; Sakai, O.; Iemura, M.; Atsumi, I.; Wada, T.; Sakaki, H. *Exp. Eye Res.* **2010**, *91*, 85−89. (c) Morita, K.; Urabe, K.; Moroi, Y.; Koga, T.; Furue, M. *J. Dermatol.* **2002**, *29*, 709−712. (d) Protzko, E. E.; Gomes, P. J.; Williams, J. I.; Gow, J. A.; McNamara, T. R. *J. Allergy Clin. Immunol.* **2009**, *123*, S50−58. (e) Simons, E. R.; Simons, K. J. *J. Allergy Clin. Immunol.* **2011**, *128*, 1139−1341.

(6) Truppo, M. D.; Pollard, D.; Devine, P. *Org. Lett.* **2007**, *9*, 335−338.

(7) Mahdy, A. M.; Webster, N. R. *Anaesth. Crit. Care. Pa.* **2017**, *18* (4), 210.

(8) Sun, Z.; Li, G.; Ilie, A.; Reetz, M. T. *Tetrahedron Lett.* **2016**, *57*, 3648−51.

(9) Wang, B.; Zhou, H.; Lu, G.; Liu, Q.; Jiang, X. *Org. Lett.* **2017**, *19*, 2094−7.

(10) Chen, C.; Reamer, R. A.; Chilenski, J. R.; McWilliams, C. J. *Org. Lett.* **2003**, *5*, 5039−42.

(11) Kamitori, S.; Iguchi, A.; Ohtaki, A.; Yamada, M.; Kita, K. *J. Mol. Biol.* **2005**, *352*, 551−558.

(12) Li, H.; Zhu, D.; Hua, L.; Biehl, E. R. *Adv. Synth. Catal.* **2009**, *351*, 583−588.

(13) Xu, J.; Zhou, S.; Zhao, Y.; Xia, J.; Liu, X.; Xu, J.; He, B.; Wu, B.; Zhang, J. *Chem. Eng. J.* **2017**, *316*, 919−27.

(14) Agudo, R.; Roiban, G. D.; Reetz, M. T. *J. Am. Chem. Soc.* **2013**, *135*, 1665−8.

(15) Zhu, D.; Yang, Y.; Buynak, J. D.; Hua, L. *Org. Biomol. Chem.* **2006**, *4*, 2690−5.

(16) Zhu, D.; Yang, Y.; Majkowicz, S.; Pan, T. H.; Kantardjieff, K.; Hua, L. *Org. Lett.* **2008**, *10*, 525−528.

(17) Reetz, M. T. *J. Am. Chem. Soc.* **2013**, *135*, 12480−96.

(18) Prelog, V. *Pure Appl. Chem.* **1964**, *9*, 119−130.

(19) Zhu, D.; Hua, L. *Pure Appl. Chem.* **2010**, *82*, 117−128.

(20) Li, Z.; Liu, W.; Chen, X.; Jia, S.; Wu, Q.; Zhu, D.; Ma, Y. *Tetrahedron* **2013**, *69*, 3561−4.

(21) Li, A.; Ye, L.; Yang, X.; Yang, C.; Gu, J.; Yu, H. *Chem. Commun. (Cambridge, U. K.)* **2016**, *52*, 6284−7.

(22) Li, G.; Wang, J.; Reetz, M. T. *Bioorg. Med. Chem.* **2018**, *26*, 1241−51.

(23) Directed evolution for engineering enzyme enantioselectivity: (a) Jaeger, K. E.; Eggert, T. *Curr. Opin. Biotechnol.* **2004**, *15*, 305−313. (b) Williams, G. J.; Woodhall, T.; Farnsworth, L. M.; Nelson, A.; Berry, A. *J. Am. Chem. Soc.* **2006**, *128*, 16238−47. (c) Reetz, M. T.; Bocola, M.; Wang, L.; Sanchis, J.; Cronin, A.; Arand, M.; Zou, J.; Archelas, A.; Bottalla, A.; Naworyta, A.; Mowbray, S. L. *J. Am. Chem. Soc.* **2009**, *131*, 7334−43. (d) Reetz, M. T. *J. Org. Chem.* **2009**, *74*, 5767−78. (e) Giger, L.; Caner, S.; Obexer, R.; Kast, P.; Baker, D.; Ban, N.; Hilvert, D. *Nat. Chem. Biol.* **2013**, *9*, 494−498. (f) Roiban, G. D.; Reetz, M. T. *Chem. Commun. (Cambridge, U. K.)* **2015**, *51*, 2208−24. (g) Sun, Z.; Wikmark, Y.; Backvall, J. E.; Reetz, M. T. *Chem. - Eur.*

J. **2016**, *22*, 5046−54. (h) Li, A.; Ilie, A.; Sun, Z.; Lonsdale, R.; Xu, J. H.; Reetz, M. T. *Angew. Chem., Int. Ed.* **2016**, *55*, 12026−9. (i) Li, G.; Wang, J. B.; Reetz, M. T. *Bioorg. Med. Chem.* **2018**, *26*, 1241. (j) Li, G.; Furst, M.; Mansouri, H. R.; Ressmann, A. K.; Ilie, A.; Rudroff, F.; Mihovilovic, M. D.; Fraaije, M. W.; Reetz, M. T. *Org. Biomol. Chem.* **2017**, *15*, 9824−9.

(24) Sun, Z.; Lonsdale, R.; Ilie, A.; Li, G.; Zhou, J.; Reetz, M. T. *ACS Catal.* **2016**, *6*, 1598−605.

(25) (a) Agudo, R.; Roiban, G. D.; Reetz, M. T. *ChemBioChem* **2012**, *13*, 1465−73. (b) Pennacchio, A.; Sannino, V.; Sorrentino, G.; Rossi, M.; Raia, C. A.; Esposito, L. *Appl. Microbiol. Biotechnol.* **2013**, *97*, 3949−64. (c) Wechsler, C.; et al. *ChemBioChem* **2015**, *16*, 2580−4. (d) Wijma, H. J.; Floor, R. J.; Bjelic, S.; Marrink, S. J.; Baker, D.; Janssen, D. B. *Angew. Chem., Int. Ed.* **2015**, *54*, 3726−30. (e) Sun, Z.; Lonsdale, R.; Wu, L.; Li, G.; Li, A.; Wang, J.; Zhou, J.; Reetz, M. T. *ACS Catal.* **2016**, *6*, 1590−7. (f) Li, A.; Ye, L.; Yang, X.; Yang, C.; Gu, J.; Yu, H. *Chem. Commun. (Cambridge, U. K.)* **2016**, *52*, 6284−7. (g) Qin, F.; Qin, B.; Mori, T.; Wang, Y.; Meng, L.; Zhang, X.; Jia, X.; Abe, I.; You, S. *ACS Catal.* **2016**, *6*, 6135−40. (h) Ebert, M. C. C. J. C.; Pelletier, A. N. *Curr. Opin. Chem. Biol.* **2017**, *37*, 89−96. (i) Liu, J.; Kuan, Y.; Tsou, Y.; Lin, T.; Hsu, W.; Yang, M.; Lin, J.; Wang, W. *Sci. Rep.* **2018**, *8*, 2316. (j) Chen, X.; Zhang, H.; Feng, J.; Wu, Q.; Zhu, D. *ACS Catal.* **2018**, *8*, 3525−31. (k) Chen, F.-F.; et al. *ACS Catal.* **2018**, *8*, 2622−8.

(26) Patel, J. M.; Musa, M. M.; Rodriguez, L.; Sutton, D. A.; Popik, V. V.; Phillips, R. S. *Org. Biomol. Chem.* **2014**, *12*, 5905−10.

(27) Zhou, J.; Xu, G.; Han, R.; Dong, J.; Zhang, W.; Zhang, R.; Ni, Y. *Catal. Sci. Technol.* **2016**, *6*, 6320−27.

(28) Guo, P.; Bao, Z.; Ma, X.; Xia, Q.; Li, W. *Biochim. Biophys. Acta, Proteins Proteomics* **2014**, *1844*, 1486−92.

(29) Dassault Systèmes BIOVIA *Discovery Studio Modeling Environment*, Release 2017, Dassault Systèmes, San Diego, 2016.

(30) Sun, Z.; Lonsdale, R.; Li, G.; Reetz, M. T. *ChemBioChem* **2016**, *17*, 1865−72.

(31) Sun, Z.; Lonsdale, R.; Kong, X. D.; Xu, J. H.; Zhou, J.; Reetz, M. T. *Angew. Chem., Int. Ed.* **2015**, *54*, 12410−5.

(32) Marrone, L.; Viswanatha, T. *Biochim. Biophys. Acta, Protein Struct. Mol. Enzymol.* **1997**, *2*, 263−277.

(33) Acevedo-Rocha, C. G.; Ferla, M.; Reetz, M. T. *Methods Mol. Biol.* **2018**, *1685*, 87−128.

(34) Gudiukaitė, R.; et al. *Appl. Biochem. Biotechnol.* **2016**, *178*, 654.

(35) Moy, V. T.; Florin, E. L.; Gaub, H. E. *Science* **1994**, *266*, 257−9.

(36) Li, G.; Yao, P.; Gong, R.; Li, J.; Liu, P.; Lonsdale, R.; Wu, Q.; Lin, J.; Zhu, D.; Reetz, M. T. *Chem. Sci.* **2017**, *8*, 4093−9.

(37) Kyte, J.; Doolittle, R. F. *J. Mol. Biol.* **1982**, *157*, 105−132.

(38) Zamyatnin, A. A. *Annu. Rev. Biophys. Bioeng.* **1984**, *13*, 145−65.

(39) Ha, T. H.; Suh, K.; Lee, G. S. B. *Bull. Korean Chem. Soc.* **2013**, *34*, 549−552.

(40) Pennacchio, A.; Sannino, V.; Sorrentino, G.; Rossi, M.; Raia, C. A.; Esposito, L. *Appl. Microbiol. Biotechnol.* **2013**, *97*, 3949−64.

(41) (a) Klinman, J. P. *CRC Crit Rev. Biochem.* **1981**, *10*, 39−78. (b) Kitson, T. M. *Biochem. J.* **1987**, *248*, 989−991. (c) Pei, X.; Erixon, K. M.; Luisi, B. F.; Leeper, F. J. *Biochemistry* **2010**, *49*, 1727−1736. (d) Chen, X.; Shi, T.; Wang, X.; Wang, J.; Chen, Q.; Bai, L.; Zhao, Y. *ACS Catal.* **2016**, *6*, 4369−4378. (e) Shi, T.; Liu, L.; Tao, W.; Luo, S.; Fan, S.; Wang, X.; Bai, L.; Zhao, Y. *ACS Catal.* **2018**, *8*, 4323−4332.

(42) Reaction mechanism of short-chain dehydrogenases: (a) McKinley-McKee, J. S.; Winberg, J. O.; Pettersson, G. *Biochem Int.* **1991**, *5*, 879−885. (b) Jörnvall, H.; Persson, B.; Krook, M.; Atrian, S.; Gonzalez-Duarte, R.; Jeffery, J.; Ghosh, D. *Biochemistry* **1995**, *34*, 6003−6013. (c) Filling, C.; Berndt, K. D.; Benach, J.; Knapp, S.; Prozorovski, T.; Nordling, E.; Ladenstein, R.; Jörnvall, H.; Oppermann, U. *J. Biol. Chem.* **2002**, *277*, 25677−25684.

(43) (a) Maria-Solano, M. A.; Romero-Rivera, A.; Osuna, S. *Org. Biomol. Chem.* **2017**, *15*, 4122−4129. (b) Agarwal, P. K.; Webb, S. P.; Hammes-Schiffer, S. *J. Am. Chem. Soc.* **2000**, *122*, 4803−4812. (c) Billeter, S. R.; Webb, S. P.; Agarwal, P. K.; Iordanov, T.; Hammes-Schiffer, S. *J. Am. Chem. Soc.* **2001**, *123*, 11262−11272.

(44) Deng, J.; Yao, Z.; Chen, K.; Yuan, Y. A.; Lin, J.; Wei, D. *J. Biotechnol.* **2016**, *217*, 31−40.

(45) Momany, F. A.; Rone, R. *J. Comput. Chem.* **1992**, *13*, 888−900.

(46) Cornell, W.; Cieplak, P.; Bayly, C. I.; Kollman, P. A.; et al. *J. Am. Chem. Soc.* **1995**, *117*, 5179−5197.

(47) Stoll, H.; Wagenblast, G.; Preuss, H. *J. Am. Chem. Soc.* **1978**, *100* (24), 7742−7743.

(48) Ryde, U. *Proteins: Struct., Funct., Genet.* **1995**, *21*, 40−56.

(49) Chen, C.; Reamer, R. A.; Chilenski, J. R.; McWilliams, C. J. *Org. Lett.* **2003**, *5*, 5039−42.

(50) Otwinowski, Z.; Minor, W. *Methods Enzymol.* **1997**, *276*, 307−326.

(51) Adams, P. D.; Grosse-Kunstleve, R. W.; Hung, L. W.; Ioerger, T. R.; McCoy, A. J.; Moriarty, N. W.; Read, R. J.; Sacchettini, J. C.; Sauter, N. K.; Terwilliger, T. C. *Acta Crystallogr., Sect. D: Biol. Crystallogr.* **2002**, *58*, 1948−54.

(52) Emsley, P.; Cowtan, K. *Acta Crystallogr., Sect. D: Biol. Crystallogr.* **2004**, *60*, 2126−32.